Published in final edited form as:
Anal Chem. 2012 March 20; 84(6): 2955–2960. doi:10.1021/ac300100b.

Online coupling of digital microfluidic devices with mass spectrometry detection using an eductor with electrospray ionization

Christopher A. Baker and **Michael G. Roper***
Department of Chemistry and Biochemistry, Florida State University, 95 Chieftain Way, Tallahassee, FL 32306

Abstract

MS detection coupled with digital microfluidic (DMF) devices has only been demonstrated in an off-line manner using matrix assisted laser desorption ionization. In this work, an eductor is demonstrated which facilitated online coupling of DMF with electrospray ionization MS detection. The eductor consisted of a transfer capillary, a standard ESI needle, and a tapered gas nozzle. As a pulse of N_2 was applied to the nozzle, a pressure differential was induced at the outlet of the ESI needle that pulled droplets from the DMF, past the ESI needle, and into the flow of gas exiting the nozzle, allowing detection by MS. Operating position, ionization potential, and N_2 pressure were optimized, with the optimum ionization potential and N_2 pressure found to be 3206 V and 80 psi, respectively. Online MS detection was demonstrated from both open and closed DMF devices using 2.5 μL and 630 nL aqueous droplets, respectively. Relative quantitation by DMF-MS was demonstrated by mixing droplets of caffeine with droplets of theophylline on an open DMF device, and comparing the peak area ratio obtained to an on-chip generated calibration curve. This eductor-based method for transferring droplets has the potential for rapid, versatile, and high throughput microfluidic analyses.

Keywords

electrowetting; Venturi; droplet; atmospheric pressure ionization

Introduction

Digital microfluidics (DMF) is a lab-on-a-chip format where discreet droplets are manipulated on an array of patterned electrodes to accomplish complex tasks. DMF devices operate by electrowetting, in which the wetting of a hydrophobic dielectric surface can be reversibly affected by application of a potential between electrodes embedded below the surface and a counter electrode in contact with the fluid. Precise manipulation of the wetting via actuation of electrode arrays allows sub-microliter droplets to be dispensed from larger volume reservoirs and enables merging, mixing, and splitting of such droplets to accomplish a multitude of analyses.

*Address Correspondence to: Dr. Michael G. Roper, Department of Chemistry and Biochemistry, Florida State University, 95 Chieftain Way, Tallahassee, FL 32306, Ph 850-644-1846, Fx 850-644-8281, roper@chem.fsu.edu.

Associated Content
Supporting Information
Videos of device operation and ANOVA tables are available free of charge via the internet at http://pubs.acs.org

Many of the benefits of DMF devices result from the small, discreet droplet volumes and the versatility of analyses that can be performed in the digital regime. The utility of discreet droplets in chemical analysis has been demonstrated in both flow-based systems[1] and in DMF format[2–4] as isolated reaction vessels[5,6] and isolated sample storage vessels.[7] Sampling in the form of droplets allows for increased temporal[8,9] and spatial[10] resolution, while the small volume of these droplets maintains high concentrations in sample-limited analyses[11] and reagent-limited reactions.[12] Performing chemical analysis in the digital regime involves combining discreet packets (droplets) of information (analytes and reagents) with a finite number of operations (droplet generation, merging, mixing and splitting) to accomplish a wide variety of analytical tasks. In this way, digital microfluidic devices are analogous to digital electronics in that they offer similar versatility from a limited number of basic tools and operations.

While the use of small volume droplets lends benefits to DMF analyses, it also poses a challenge to many traditional detection methods. As with other microfluidic formats, this challenge can be addressed by employing fluorescence detection,[13,14] however this detection scheme limits the types of analyses and the amount of information that can be attained. Mass spectrometry (MS) offers a more information-rich approach to detection, and while multiple instances of offline coupling of DMF with matrix assisted laser desorption ionization (MALDI) have been reported,[15,16] reports of electrospray ionization (ESI) sources for DMF devices are fewer.[17] A challenge to integrating the two methods is that the droplets on a DMF device are unconfined and at ambient pressure, which makes it difficult to introduce them to ESI without a pressure-assisted mechanism. Previous methods have interfaced segmented droplets from microfluidic devices, but these methods utilized pressure-induced transport to deliver these droplets to the MS.[18,19]

Another challenge with online coupling is that the typical operating voltages for DMF and ESI are dissimilar, with DMF devices operating with AC voltages[20, 21] and ESI with high DC voltages. Ambient desorption ionization methods such as desorption electrospray ionization (DESI)[22] and direct analysis in real time (DART)[23] may be amenable to online detection from DMF devices, however these methods would not be effective for ionizing droplets in closed DMF devices and would not easily allow analysis of the entire droplet volume. Additionally, integration of ESI sources with DMF devices would allow online detection, improving the versatility and throughput of DMF analyses.

A technology capable of transferring droplets from the DMF device to the ion source is needed to decouple AC and DC voltage operation while allowing online MS detection from DMF devices. An eductor is a device that uses the flow of one fluid to entrain the flow of another. Eductors operate by the Venturi effect as described by the Bernoulli principle, and are a mature technology appearing in a wide range of applications,[24–26] however this common method of fluid control is rarely employed on microfluidic devices. In this work, an eductor with an integrated ion source is presented to address the challenges of integrating DMF with online MS detection. A fused silica transfer capillary was used to couple the DMF device to a standard ESI needle. The ESI needle was aligned inside of a gas nozzle so that as N_2 flowed through the nozzle, a drop in pressure resulted at the outlet of the ESI needle by the Venturi effect. This pressure differential from the inlet of the transfer capillary to the outlet of the ESI needle pulled sub-microliter droplets from the surface of the DMF device, past the ESI needle, and ejected into the flow of N_2 to the MS inlet. A multivariate approach was used to optimize eductor operating position, applied ionization potential, and applied N_2 pressure. To demonstrate the versatility of coupling DMF with online MS analysis, droplets of caffeine were merged with droplets of an internal standard and peak areas of the resulting selected ion current (SIC) were used for quantification. This method of integration is simple and should be applicable to a large number of DMF analyses.

Materials and Methods

Materials

Caffeine, theophylline and Met-Arg-Phe-Ala peptide (MRFA) were purchased from Sigma-Aldrich (St. Louis, MO). Acetic acid was purchased from EMD Chemicals Inc. (Gibbstown, NJ). SU8-3035 was purchased from Microchem Corporation (Newton, MA). Teflon AF solution was purchased from DuPont (Wilmington, DE). EGC-1700 was purchased from 3M (St. Paul, MN).

Eductor fabrication and operation

High density polyethylene tubing with an inner diameter of 3 mm was heat drawn to an outlet diameter of 1.5 mm to form the nozzle of the eductor. A regulator controlled the pressure from the N_2 tank. Timing of N_2 delivery to the nozzle was controlled by 9 computer-controlled solenoid valves (model A00SC232P, Parker Hannifin Corp., Cleveland, OH) with the outlets connected together. The transfer line from the DMF device was a 10 cm × 150 μm o.d. × 100 μm i.d. fused silica capillary (Polymicro Technologies, Phoenix, AZ) while a standard ESI needle (P/N 00950-00951, Thermo Fisher Scientific Inc., Waltham, MA) was used. Ionization potential was applied by a high voltage DC power supply (model 6AA12-P4, Ultravolt, Ronkonkoma, NY) controlled by software written in Labview 8.5 (National Instruments, Austin, TX).

DMF Device Fabrication

Electrode patterns were fabricated on chrome photomask blanks (Telic Co., Valencia, CA) by photolithography and chrome etching. The electrode pattern consisted of a 5 mm × 5 mm reservoir electrode segmented into two parts, and six working electrodes for droplet dispensing and delivery to the transfer capillary. Electrodes were connected to electrical contact pads at the edge of the device designed to interface with a card edge connector (model 3666-0000, 3M, St. Paul, MN). To improve the uniformity of dielectric coatings, patterned electrodes were subjected to two minutes of plasma oxidation (model PDC-32G, Harrick Plasma, Ithaca, NY) prior to spin coating SU8-3035 at 7000 rpm for 40 s. The dielectric thickness was 19.7 ± 0.9 μm as measured by a profilometer (P-15, KLA-Tencor, Milpitas, CA). Coated devices were baked for 5 min at 65 °C followed by 5 min at 95 °C before being exposed to 25 s of UV radiation at an intensity of 20 mW cm^{-2} using a collimated UV source (OAI, San Jose, CA). The devices were left overnight to complete the curing of SU8. Cured devices were spin coated with a 1% solution of Teflon AF 1600 at 2500 rpm for 20 s then baked for 5 min at 75 °C to evaporate the solvent. The coated surface was then quickly passed over a gas burner several times (< 1 s per pass) to reduce surface roughness.

Grounding electrodes for open DMF devices were fabricated by dip coating 30 gauge tin plated copper wire in EGC-1700 electronics coating. The grounding electrodes were placed approximately 100 μm to the side of the working electrodes which allowed continuous contact with the droplets. Cover slides for closed DMF devices consisted of 25 mm × 75 mm ITO-coated glass slides (P/N 576352, Sigma-Aldrich). The ITO surface was coated with Teflon AF by the same procedure described above, except a final baking step of 15 min at 330 °C was performed rather than passing the devices over a gas flame. Closed devices were assembled by spacing the ITO cover slides 175 μm from the DMF surface using a gasket made from two layers of blue low tack tape (Semiconductor Equipment Corporation, Moorpark, CA).

DMF device operation

Droplet actuation was achieved by applying 175 – 225 V_{rms} at 1 kHz to the patterned electrodes while the 30 gauge tin plated copper wire or ITO cover slide was grounded. The control voltage was generated by passing the output of a function generator (model 4003A, B&K Precision Corporation, Yorba Linda, CA) through a high voltage amplifier (model 601C, TREK, Inc., Medina, NY). Voltage application was controlled using computer-controlled 12V relays (CK1601A, Carl's Electronics, Oakland, CA) interfaced to the DMF device with a card edge connector. Droplet volumes in closed DMF devices were determined from digital images of droplet generation using ImageJ software.[27]

Mass spectrometry parameters

Mass spectra were collected using a Finnigan LCQ Duo (Thermo Fisher Scientific Inc., Waltham, MA). Unless otherwise noted, selected ion monitoring (SIM) was performed over a 10 m/z range centered at the indicated ion of interest. Selected ion currents (SIC) were taken from the SIM data using a 1 m/z window centered on the ion of interest. For measurement of caffeine:theophylline ratios, the mass analyzer was scanned from 175 – 200 m/z, and the SIC of each compound using a 1 m/z window was used for each compound. The ratio of the areas of these SIC traces was then taken. The MS instrument was operated with a capillary temperature of 200 °C and a 10 ms ion injection time. Ionization voltages ranged from 0 to +6 kV DC, and were applied using a computer-controlled high voltage power supply as mentioned previously.

Optimization and characterization experiments

Design Expert 7 software (StatEase, Minneapolis, MN) was used to develop the experimental design and to perform all statistical analyses. Four experimental factors were varied over three levels each, as described in Table 1. A Box-Behnken experimental design was used to reduce the 64 possible combinations to 29 experiments (including 5 replicates of the median condition, x = 5 mm, y = 37.5 mm, P = 60 psi, and V = 3000 V). Each of the four factors was then fit to a polynomial model with the general form:

$$R=\beta_i+x+y+V+P+xy+xV+xP+yV+yP+VP+x^2+y^2+V^2+P^2+xyV+xyP+xVP+yVP+x^2y+x^2V+x^2P+xy^2+xV^2+xP^2+y^2V+y^2P+yV^2+yP^2+V^2P+VP^2+x^3+y^3+V^3+P^3+E_i \quad (1)$$

where R was the response (average peak area or peak area RSD), β_i was the model coefficient, E_i was the residual error, x was the position off-axis relative to the MS inlet, y was the distance from the MS inlet, V was the ionization potential, and P was the applied N_2 pressure. Analysis of variance (ANOVA) was used to partition the total variation in the data into the variations due to the four experimental factors and the variation due to random error. These components were used to calculate an F-value, which was compared to a tabulated F-distribution to generate a p-value. The p-value described the probability that a variation resulted from error rather than from an experimental factor. When $p < 0.05$, the effect of that factor was considered to be significant. Model reduction, which pooled non-significant terms ($p > 0.10$) with the residual error by backward elimination regression, was applied to find the best fit for each response. The final reduced model for each response was described by the following equations:

$$\text{Log(peak area)}=\beta_1+x+V+P \quad (2)$$

$$\text{RSD of peak area}=\beta_2+x+y+V+P+VP+y^2 \quad (3)$$

ANOVA tables for each of the reduced models above are given in Tables S1 and S2 in the supporting information.

Unless otherwise stated, all signals were quantified by integrating the area under the SIC traces, and the analyte was 2.5 μL aqueous droplets of 10 μg mL^{-1} MRFA (m/z = 524.3) acidified with 1% acetic acid.

Semi-quantitative analysis was performed with 2.5 μL aqueous droplets containing caffeine concentrations of 5 – 250 μg mL^{-1}, with theophylline (m/z = 181.1, $[M+H]^+$) as an internal standard at a final concentration of 100 μg mL^{-1}.

Results

Online MS detection from DMF devices is an attractive option for high throughput and parallel analyses with information rich detection. Coupling DMF to ESI-MS is challenging because it is difficult to introduce a pressure-assisted mechanism to droplets that are at ambient pressure and not confined by fluidic channels. Additionally, the voltage regimes of DMF (typically hundreds of volts AC) and ESI (typically kilovolts DC) are difficult to integrate into a single electronic system. To address these challenges, we have developed a microfluidic eductor that transfers DMF droplets to an ESI source and subsequently into an MS instrument for detection.

Design and principles of operation

The eductor, illustrated in Figure 1A, consisted of a transfer capillary, a standard ESI needle, and a tapered gas nozzle. The transfer capillary coupled the DMF device to the ESI needle, with the outlet of the transfer capillary recessed 2 mm from the outlet of the ESI needle. The ESI needle was aligned coaxially inside the gas nozzle, with the outlet of the needle recessed 1 mm from the outlet of the gas nozzle. With this configuration it was possible to introduce sub-microliter droplets into the mass spectrometer by applying a 15 s pulse of N_2 to the nozzle. As the gas pulse passed the ESI needle, a drop in pressure was induced at the outlet of the ESI needle, which pulled droplets from the DMF device, through the transfer capillary, past the ESI needle, and into the flow of gas exiting the nozzle.

The device was easily coupled to DMF devices of both closed and open configurations, provided that the gap spacing of the closed DMF devices was greater than the 150 μm outer diameter of the transfer capillary. Video demonstrations of the eductor operating with both open and closed DMF devices can be found in the supporting information. Droplet volumes of 630 ± 90 nL were successfully transferred from closed DMF devices, whereas open DMF devices were loaded with 2.5 μL droplets by pipette. In either case, droplets from the DMF device resulted in peaks in the SIC that were rectangular in shape with the duration of the signal proportional to the volume of the droplet being transferred (Figure 1B). The RSD of the ion current magnitude from a single peak was higher than 20%, but the areas of the SIC produced from droplets of identical composition and volume were less than 10% RSD.

MS detection of small molecules, peptides, and proteins were all possible with this system. The present studies focused on detection of small molecules and peptides because biomolecule adsorption on the surface of the DMF device, a well known phenomenon,[28] hindered the analysis of proteins (data not shown). This carryover does not limit the efficacy of the system, however, since methods exist to address protein carryover on DMF devices.[29]

Performance characterizations and optimization

The eductor was positioned in front of the MS inlet on a two axis positioning stage, and a multivariate approach was used to characterize the performance of the eductor as a function

of four factors: x-position (off-axis position relative to the MS inlet), y-position (distance from the MS inlet), applied ionization potential, and applied N_2 pressure. Table 1 shows the levels over which each of these factors was tested. A Box-Bhenken experimental design, similar to those described previously,[30, 31] was used to reduce the total number of experiments needed. In each experiment, the average SIC peak area from 5 replicate droplets and the RSD of the replicate peak areas were the measured responses. ANOVA was used to identify statistically significant relationships between the factors and these responses.

The peak area response was fit to a model ($p < 0.0001$) where the log of peak area varied linearly with respect to x-position ($p < 0.0001$) and ionization voltage ($p = 0.0320$). Neither y-position nor applied N_2 pressure affected peak area in a statistically significant manner. Figure 2 illustrates the relationship between the log of peak area and both x-position and applied ionization potential. Not surprisingly, peak area increased with increasing ionization potential and decreased as the eductor was moved off-axis with respect to the MS inlet. The maximum experimentally observed peak area occurred at x = 0 mm and at an ionization potential of 5000 V. The factors found to be insignificant in this model, y-position and N_2 pressure, both play a role in the desolvation of ions prior to MS detection. The lack of a statistically significant relationship between these factors and peak area suggests that either sufficient desolvation occurred even at low N_2 pressure and at short distances from the MS inlet, or that desolvation did not play a significant role in changing the SIC peak areas. Further studies will be required to completely understand the role these factors have on ion desolvation in this system.

Peak area reproducibility followed a more complex trend, with the RSD of SIC peak areas fitting a quadratic model ($p = 0.0030$). In this model, significant relationships were found for both applied N_2 pressure ($p = 0.0063$) and the square of y-position ($p = 0.0027$). The first order y-position term was not statistically significant ($p = 0.837$) but was retained in the model to maintain hierarchy with the y^2 term. Figure 3 shows the relationship between peak area RSD and both y-position and applied N_2 pressure. The dependence of RSD on y^2 is evident by the parabolic shape of the response surface, with the minimum RSD found at a y-position of 37.5 mm at each value of N_2 pressure. Peak area RSD decreased with increasing N_2 pressure, with the highest experimentally observed peak area reproducibility (5% RSD) at the highest N_2 pressure (80 psi). As discussed previously, N_2 pressure and y-position were insignificant factors when attempting to increase the average peak area, suggesting that droplet desolvation did not play a significant role in peak area. But, due to their significance in this study, the shape and mechanics of plume generation and ion desolvation appear to strongly influence the reproducibility of the SIC peak areas. Previous reports have looked at plume shape and mechanics in similar ionization sources,[32] but we felt a peak area precision of 5% was sufficient. Relationships of borderline significance were x-position ($p = 0.0794$) and the product of N_2 pressure and ionization potential ($p = 0.0903$). Ionization potential was not found to be statistically significant ($p = 0.232$), but was retained in the model to preserve hierarchy. Preliminary studies indicated that modulating N_2 pressure was also an effective method for affecting the rate of droplet transfer from the DMF device to the MS detector, with decreased N_2 pressure leading to slower transfer speeds (data not shown). While this may be useful in tuning an analysis to particularly small or large volume droplets, it should be noted that doing so would have an impact on peak area reproducibility.

The performance characterizations described above were used to identify optimum operating conditions. Two equally weighted optimization goals were defined: 1) maximizing the SIC peak area, and 2) minimizing peak area RSD. A desirability function scored how closely the response met the optimization goals, with a desirability score of 1 indicating that the response was in perfect agreement with the optimization goals.[33] Figure 4 shows a spatial plot of the desirability score as a function of x- and y-position at the identified optimal N_2

pressure and ionization potential. A maximum desirability score of 0.919 is predicted when the eductor is positioned on-axis with the MS inlet, at a distance of 37.5 mm, with an ionization potential of 3206 V and an N_2 pressure of 80.0 psi. At these conditions, the experimentally observed average peak area was 26308 arbitrary units with an RSD of 5%, which agreed with the results predicted by the model of an average peak area of 26440 arbitrary units and an RSD of 3% (Figure 4B).

DMF-MS analysis

Preliminary studies suggested that peak area in the SIC was an effective means for quantifying signal in these studies, and thus motivated the investigation of peak area in the device characterizations described above. To validate the use of SIC peak area in DMF-MS analyses, a semi-quantitative DMF-MS analysis was performed.

The ability to rapidly mix droplets makes DMF devices a promising platform for relative quantitation by MS because analyte-containing droplets can be combined with internal standards prior to analysis. Relative quantitation of caffeine from aqueous droplets on a DMF device is illustrated in Figure 5. Droplets containing premixed solutions of caffeine with theophylline internal standard were transferred from the DMF device to the MS by the eductor. Ratios of the caffeine/theophylline peak areas (Figure 5A, squares) gave a calibration curve with a linear range of 5 – 250 μg mL^{-1} (12.5 – 625 ng per droplet) and a best fit line of $y = 0.0159 x + 0.0237$ ($R^2 = 0.999$). Under these conditions, caffeine was detected regularly at concentrations of 1 μg/mL (2.5 ng per droplet), but 10-fold lower concentrations were not. Shown in the inset of Figure 5A are examples of the SIC traces obtained at two points within the calibration curve. The blue trace is the SIC of caffeine (m/z = 195) and the black trace is from theophylline (m/z = 181). Aqueous droplets spiked with caffeine were combined on the DMF device with droplets containing theophylline (Figure 5B) and allowed to mix by diffusion. The resulting relative peak areas agreed well with the calibration curve (Figure 5A, diamonds), and validated the use of relative peak areas as a means of quantifying DMF droplet contents by online MS detection.

Conclusion

Coupling of DMF devices to ESI-MS allows the advantages of digital analyses with the information-rich detection offered by MS. The eductor-integrated ionization method presented here facilitates online MS detection from open or closed DMF devices in two ways. First, the eductor imparts a motive force to the droplets to deliver them to the ESI needle addressing the challenge associated with ambient and unconfined droplets. Ambient ionization mass spectrometry methods, such as DESI or DART, could be used to analyze droplets from open DMF devices, but it would be a challenge to analyze droplets from closed DMF devices. Secondly, the eductor is designed to remove droplets from the DMF device, which allows the high DC ionization potential to be decoupled from the voltage scheme of the DMF device permitting MS analysis while movement of other droplets on the DMF can continue uninterrupted. Droplet removal has the additional benefits of allowing detection from the entire droplet volume, and of clearing droplets from the device to allow high throughput or highly paralleled analyses.

DMF devices achieve complex tasks from a limited number of operations, which makes this technology ideally suited for highly versatile analysis systems. Online MS detection from DMF devices complements this versatility well, since it will allow optimization, calibration, and analytical measurements to be performed within the same experiment, without taking the DMF device offline.

Supplementary Material

Refer to Web version on PubMed Central for supplementary material.

Acknowledgments

This work was supported in part by a grant from the National Institutes of Health (R01 DK080714). The authors would like to thank the Florida Department of Agriculture for donating the MS instrument used in this work and Dr. Christopher Hendrickson for advice on maintaining the instrument.

References

1. Teh SY, Hung LH, Lee AP. Lab Chip. 2008; 8:198–220. [PubMed: 18231657]
2. Pollack MG, Shenderov AD, Fair RB. Lab Chip. 2002; 2:96–101. [PubMed: 15100841]
3. Cho SK, Moon HJ, Kim CJ. J Microelectromech S. 2003; 12:70–80.
4. Fair RB. Microfluid Nanofluid. 2007; 3:245–281.
5. Song H, Chen DL, Ismagilov RF. Angew Chem Int Edit. 2006; 45:7336–7356.
6. Luk VN, Wheeler AR. Anal Chem. 2009; 81:4524–4530. [PubMed: 19476392]
7. Huebner A, Srisa-Art M, Holt D, Abell C, Hollfelder F, Demello AJ, Edel JB. Chem Comm. 2007; 12:1218–1220. [PubMed: 17356761]
8. Easley CJ, Rocheleau JV, Head WS, Piston DW. Anal Chem. 2009; 81:9086–9095. [PubMed: 19874061]
9. Song H, Ismagilov RF. J Am Chem Soc. 2003; 125:14613–14619. [PubMed: 14624612]
10. Chen D, Du WB, Liu Y, Liu WS, Kuznetsov A, Mendez FE, Philipson LH, Ismagilov RF. P Natl Acad Sci USA. 2008; 105:16843–16848.
11. Beer NR, Hindson BJ, Wheeler EK, Hall SB, Rose KA, Kennedy IM, Colston BW. Anal Chem. 2007; 79:8471–8475. [PubMed: 17929880]
12. Gosalia DN, Diamond SL. P Natl Acad Sci USA. 2003; 100:8721–8726.
13. Miller EM, Wheeler AR. Anal Chem. 2008; 80:1614–1619. [PubMed: 18220413]
14. Miller EM, Ng AHC, Uddayasankar U, Wheeler AR. Anal Bioanal Chem. 2011; 399:337–345. [PubMed: 21057776]
15. Wheeler AR, Moon H, Kim CJ, Loo JA, Garrell RL. Anal Chem. 2004; 76:4833–4838. [PubMed: 15307795]
16. Wheeler AR, Moon H, Bird CA, Loo RRO, Kim CJ, Loo JA, Garrell RL. Anal Chem. 2005; 77:534–540. [PubMed: 15649050]
17. Jebrail MJ, Yang H, Mudrik JM, Lafreniere NM, McRoberts C, Al-Dirbashi OY, Fisher L, Chakraborty P, Wheeler AR. Lab Chip. 2011; 11:3218–3224. [PubMed: 21869989]
18. Pei J, Li Q, Lee MS, Valaskovic GA, Kennedy RT. Anal Chem. 2009; 81:6558–6561. [PubMed: 19555052]
19. Fidalgo LM, Whyte G, Ruotolo BT, Benesch JLP, Stengel F, Abell C, Robinson CV, Huck WTS. Angew Chem Int Edit. 2009; 48:3665–3668.
20. Wang KL, Jones TB, Raisanen A. Lab Chip. 2009; 9:901–909. [PubMed: 19294300]
21. Shih SCC, Fobel R, Kumar P, Wheeler AR. Lab Chip. 2011; 11:535–540. [PubMed: 21038034]
22. Takáts Z, Wiseman JM, Cooks RG. J Mass Spectrom. 2005; 40:1261–1275. [PubMed: 16237663]
23. Cody RB, Laramée JA, Durst HD. Anal Chem. 2005; 77:2297–2302. [PubMed: 15828760]
24. Rodes TW. Ind Eng Chem. 1951; 43:A97–A98.
25. Labelle MA, Juteau P, Jolicoeur M, Villemur R, Parent S, Comeau Y. Water Res. 2005; 39:3409–3417. [PubMed: 16023699]
26. Reed RJR, Forrest IS. J I Brewing. 1986; 92:370–378.
27. Abramoff MD, Magelhaes PJ, Ram SJ. Biophotonics International. 2004; 11:36–42.
28. Yoon J, Garrell RL. Anal Chem. 2003; 75:5097–5102.
29. Luk VN, Mo GCH, Wheeler AR. Langmuir. 2008; 24:6382–6389. [PubMed: 18481875]

30. Baker CA, Roper MG. J Chromatogr A. 2010; 1217:4743–4748. [PubMed: 20730040]
31. Lomasney AR, Guillo C, Sidebottom AM, Roper MG. Anal Bioanal Chem. 2009; 394:313–319. [PubMed: 19189083]
32. Derringer G, Suich R. J Qual Technol. 1980; 12:214–219.
33. Wang R, Allmendinger P, Zhu L, Grohn AJ, Wenger K, Frankevich V, Zenobi R. J Am Soc Mass Spectrom. 2011; 22:1234–1241. [PubMed: 21953106]

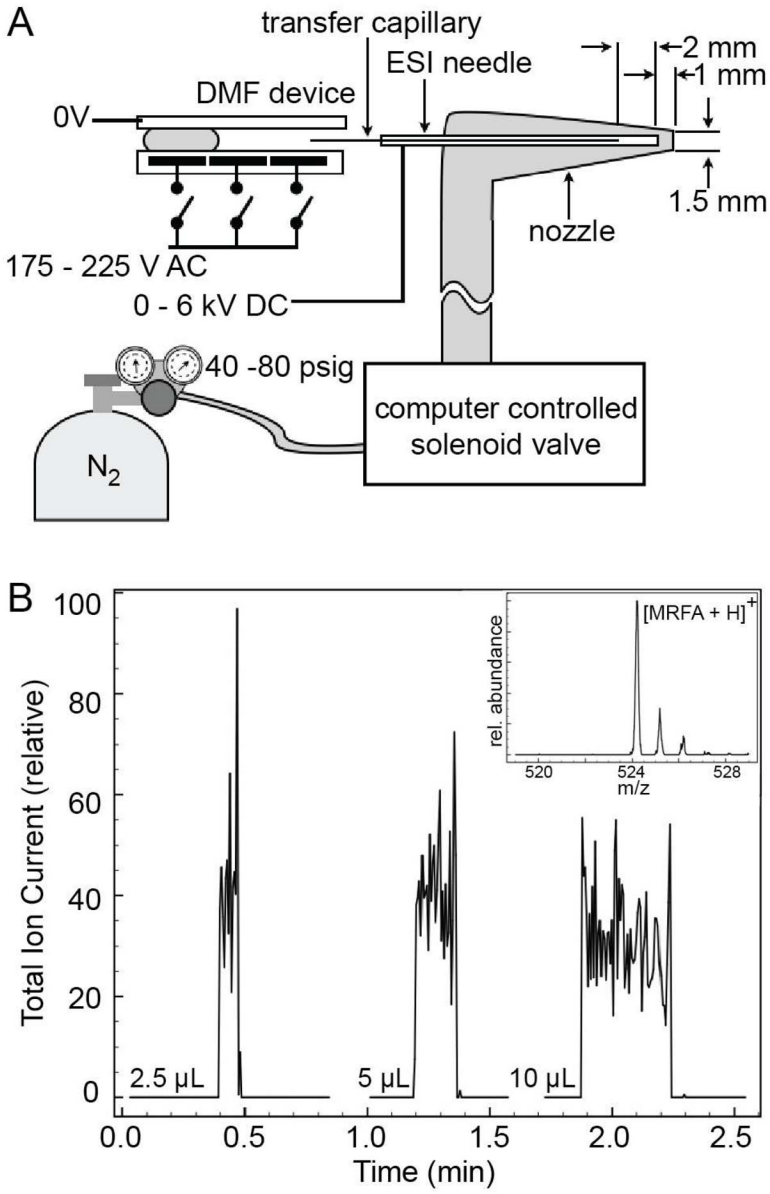

Figure 1. Microfluidic eductor operation

A. A schematic representation of the eductor is shown, illustrating the configuration of the transfer capillary, ESI needle, and gas nozzle. Gas flow in the nozzle induced a pressure differential between the outlet of the ESI needle and inlet of the transfer capillary, which allowed droplets from the DMF device to be transferred to the MS. The inset shows the eductor coupled to a closed DMF device. **B.** The SIC traces produced when 2.5, 5, and 10 µL droplets of MRFA peptide were transferred from an open DMF device via the eductor-integrated ion source into the MS are shown. The areas of the resulting signals were proportional to droplet volume. The inset shows the mass spectrum resulting from the summation of all 15 m/z scans from the 2.5 µL droplet.

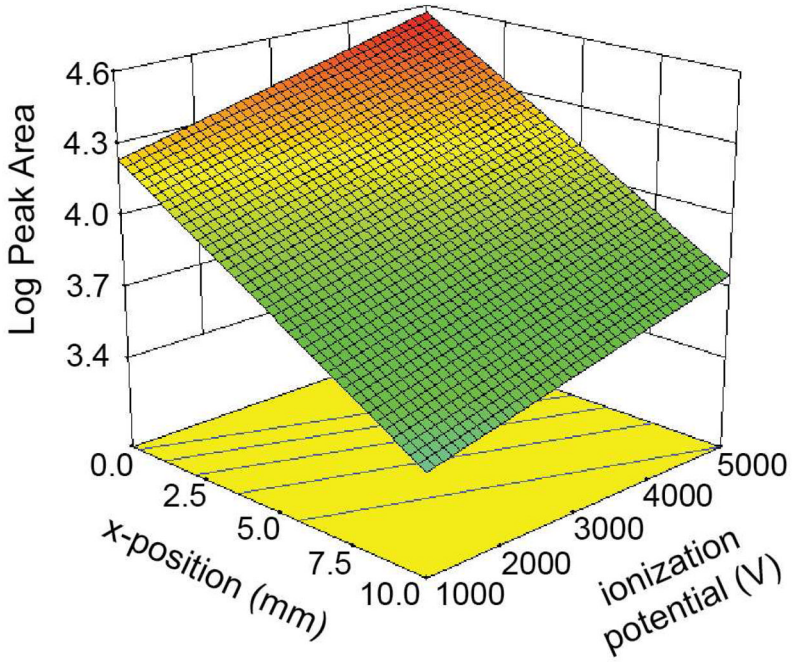

Figure 2. Peak area response surface map

Results of ANOVA show that the log of peak area followed a linear trend with respect to ionization potential and x-position, with increasing peak area observed at increasing ionization potential, and decreasing peak area observed as the eductor was positioned off-axis with respect to the MS inlet. Neither y-position nor N_2 pressure was found to significantly affect average peak area.

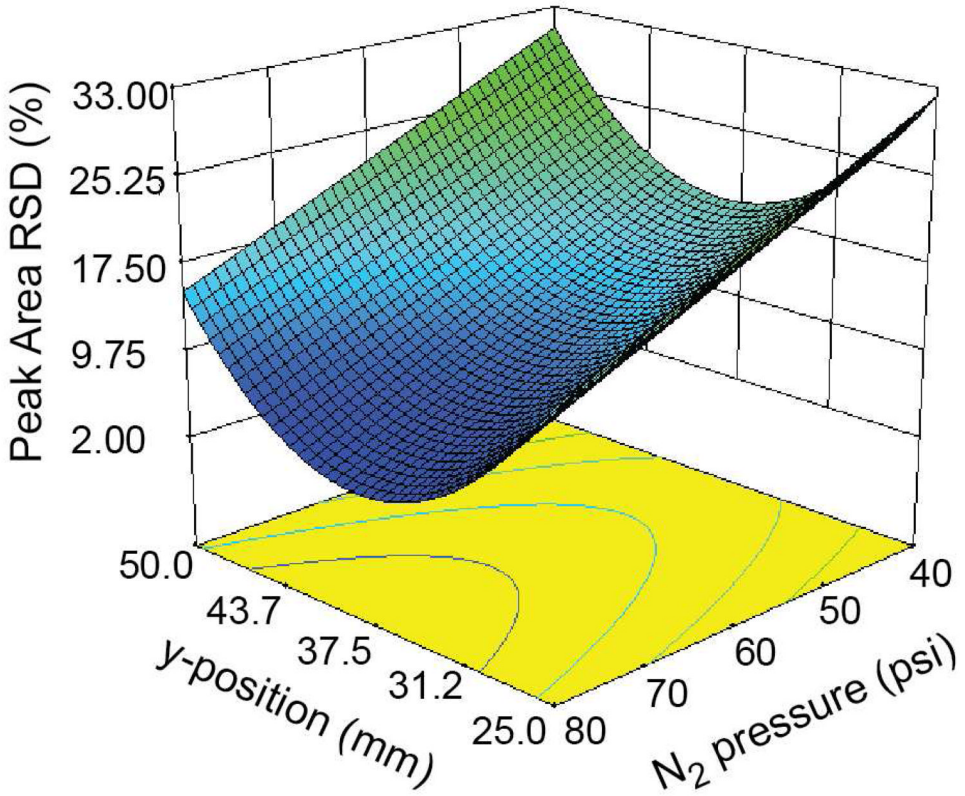

Figure 3. Peak area RSD response surface map

The RSD of peak area followed a quadratic model, with the best reproducibility observed at y = 37.5 mm and 80 psi N_2 pressure. Data is shown at x = 0 and an ionization potential of 3206 V.

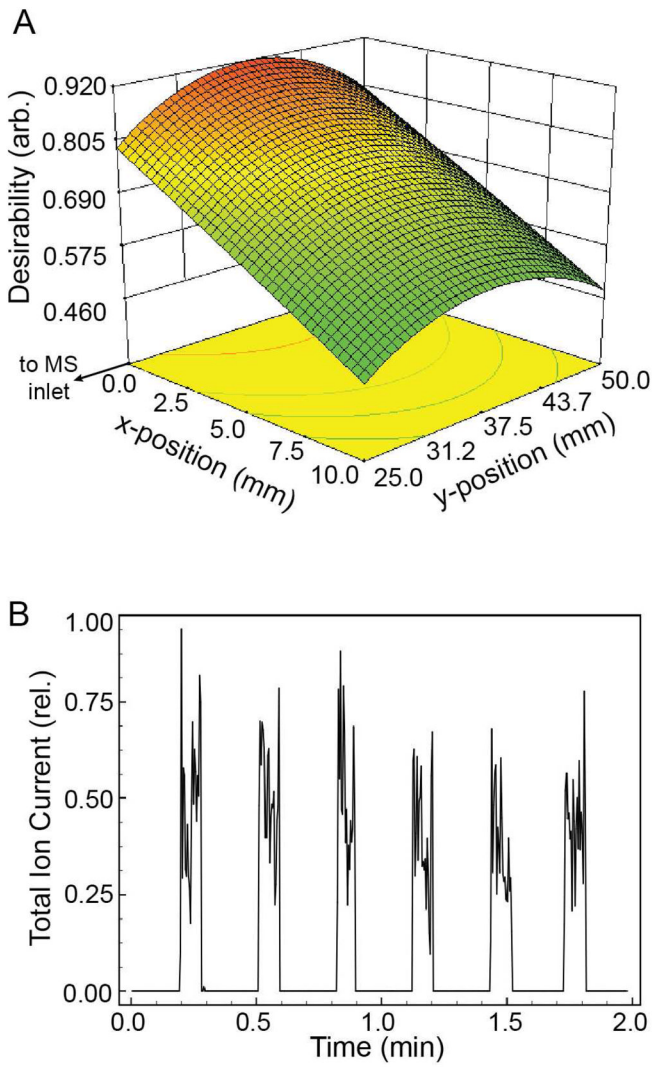

Figure 4. Optimization of eductor operating conditions

A. Optimization targets of maximum peak area and minimum peak area RSD resulted in a maximum desirability at x = 0 and y = 37.5 mm. The desirability plot is shown at the optimal ionization potential and N_2 pressure of 3206 V and 80 psi, respectively. **B.** Repeated droplet transfer at the optimum operating conditions showed reproducible SIC peak areas (RSD = 5%).

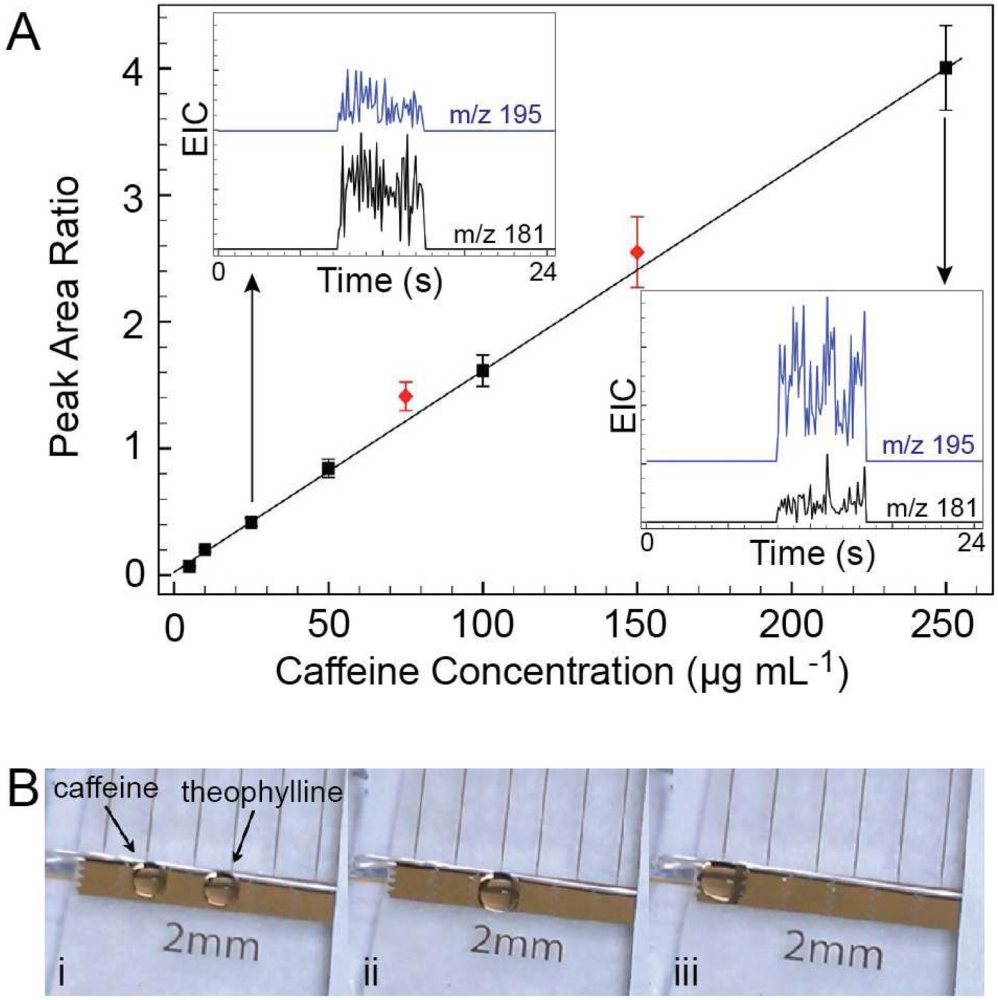

Figure 5. Relative quantitation of caffeine from a DMF device

A. 2.5 μL droplets of premixed standard solutions (squares) containing caffeine (5 – 250 μg mL^{-1}) and theophylline (100 μg mL^{-1}) were delivered to the mass spectrometer through the eductor. The ratio of the SIC peak areas for caffeine and theophylline are plotted as a function of caffeine concentration. Insets show typical SIC traces of caffeine (blue traces) and theophylline (black traces) at 25 and 250 μg mL^{-1} caffeine concentrations. **B.** Droplets containing different caffeine concentrations were mixed on-chip with droplets of theophylline internal standard and delivered to the mass spectrometer. The ratio of the extracted ion currents for caffeine and theophylline were plotted in **A** as red diamonds.

Table 1

Experimental factors and levels

Factors	Level (−)	Level (0)	Level (+)
x-position (mm)	0	5	10
y-position (mm)	17	27	37
ionization potential (V)	1000	3000	5000
N_2 pressure (psi)	40	60	80